The Astrophysical Journal Letters, 942:L35 (10pp), 2023 January 10 https://doi.org/10.3847/2041-8213/acae99

Missing for 20 yr: MeerKAT Redetects the Elusive Binary Pulsar M30B

Vishnu Balakrishnan[1], Paulo C. C. Freire[1], S. M. Ransom[2], Alessandro Ridolfi[1,3], E. D. Barr[1], W. Chen[1], Vivek Venkatraman Krishnan[1], D. Champion[1], M. Kramer[1,4], T. Gautam[1], Prajwal V. Padmanabh[1,5,6], Yunpeng Men[1], F. Abbate[1], B. W. Stappers[4], I. Stairs[7], E. Keane[8], and A. Possenti[3]
[1] Max-Planck-Institut fur Radioastronomie, Auf dem Hügel 69, D-53121 Bonn, Germany
[2] National Radio Astronomy Observatory, 520 Edgemont Road, Charlottesville, VA 22903, USA
[3] INAF—Osservatorio Astronomico di Cagliari, Via della Scienza 5, I-09047 Selargius (CA), Italy
[4] Jodrell Bank Centre for Astrophysics, Department of Physics and Astronomy, The University of Manchester, Manchester M13 9PL, UK
[5] Max Planck Institute for Gravitational Physics (Albert Einstein Institute), D-30167 Hannover, Germany
[6] Leibniz Universität Hannover, D-30167 Hannover, Germany
[7] Department of Physics and Astronomy, University of British Columbia, 6224 Agricultural Road, Vancouver, BC V6T 1Z1, Canada
[8] 6 School of Physics, Trinity College Dublin, University of Dublin, College Green, Dublin 2, D02 PN40, Ireland
Received 2022 November 17; revised 2022 December 21; accepted 2022 December 23; published 2023 January 12

Abstract

PSR J2140−2311B is a 13 ms pulsar discovered in 2001 in a 7.8 hr Green Bank Telescope observation of the core-collapsed globular cluster M30 and predicted to be in a highly eccentric binary orbit. This pulsar has eluded detection since then; therefore, its precise orbital parameters have remained a mystery until now. In this work, we present the confirmation of this pulsar using observations taken with the UHF receivers of the MeerKAT telescope as part of the TRAPUM Large Survey Project. Taking advantage of the beamforming capability of our backends, we have localized it, placing it $1\farcm2(1)$ from the cluster center. Our observations have enabled the determination of its orbit: It is highly eccentric ($e = 0.879$) with an orbital period of 6.2 days. We also measured the rate of periastron advance, $\dot{\omega} = 0.078 \pm 0.002$ deg yr^{-1}. Assuming that this effect is fully relativistic, general relativity provides an estimate of the total mass of the system, $M_{\rm TOT} = 2.53 \pm 0.08\,M_{\odot}$, consistent with the lightest double neutron star systems known. Combining this with the mass function of the system gives the pulsar and companion masses of $m_p < 1.43\,M_{\odot}$ and $m_c > 1.10\,M_{\odot}$, respectively. The massive, undetected companion could either be a massive white dwarf or a neutron star. M30B likely formed as a result of a secondary exchange encounter. Future timing observations will allow the determination of a phase-coherent timing solution, vastly improving our uncertainty in $\dot{\omega}$ and likely enabling the detection of additional relativistic effects, which will determine m_p and m_c.

Unified Astronomy Thesaurus concepts: Radio pulsars (1353); Globular star clusters (656)

1. Introduction

Globular clusters (GCs) are dense spheroidal arrangements of stars held together by their own gravity. Their high stellar densities (10^{3-6} pc^{-3}) enable dynamical interactions, where some of these old neutron stars (NSs)—which would have remained undetectable if located in the Galactic disk—can gain a stellar-mass companion, for example, a main-sequence (MS) star either in binary–single star encounters, or direct NS–MS encounters (Verbunt & Hut 1987; Davies & Benz 1995; Sigurdsson & Phinney 1995; Davies & Hansen 1998).

In the resulting binaries, an MS or giant star transfers mass and angular momentum to the NS. During this accretion process, commonly referred to as "recycling," thermal X-ray emission is produced due to frictional heating from the infalling matter, making these systems detectable as low-, intermediate-, or high-mass X-ray binaries depending on the mass of the donor star. In GCs, only low-mass stars are still on the MS; therefore, any X-ray binaries containing NSs are low-mass X-ray binaries (LMXBs; Clark 1975). Because low-mass MS companions evolve slowly, LMXBs are very long-lived. At the end of this process, a recycled radio pulsar (a "millisecond pulsar," or MSP, with $P < 20$ ms) emerges (e.g., Alpar et al. 1982). These systems mostly resemble the MSPs in the Galactic disk, which have a wide variety of companions (black widows, redbacks, white dwarfs (WDs), and some isolated MSPs as well); all of them are produced by unperturbed stellar evolution, and the majority have orbits with low ($e < 10^{-3}$) eccentricities (Manchester et al. 2005).[9]

These dynamical formation channels for LMXBs explain why LMXBs and MSPs are so abundant in GCs relative to the Galaxy. At the time of writing (2022 December), 272 radio pulsars in 38 GCs are known (see the GC Pulsar Catalog[10]), of which 245 (∼90%) are MSPs. Per unit stellar mass, GCs are estimated to have three orders of magnitude more LMXBs and MSPs than the Galactic disk (Clark 1975; van den Berg 2020). Some of these channels, like direct collisions of NSs with MS stars (Davies et al. 1992), can also explain some of the exotic objects found in GCs, like ultracompact X-ray binaries (Ivanova et al. 2005), see Ye et al. (2022) for a recent review. Furthermore, some dynamical interactions, like perturbations from nearby stars, explain why a significant percentage of the MSPs–WD systems in GCs have mildly eccentric orbits (Phinney 1992; Camilo & Rasio 2005; Ransom 2008).

However, the extreme stellar densities at the cores of the GCs with the highest interaction rates per binary, γ (Verbunt & Freire 2014)—especially the core-collapsed GCs—imply that stars are likely to go through repeated gravitational interactions with other stars and binaries in the core. This leads to the

[9] https://www.atnf.csiro.au/research/pulsar/psrcat/
[10] See http://www.naic.edu/~pfreire/GCpsr.html for an up-to-date count.

formation, in these GCs, of binary systems where already fully recycled MSPs acquire massive companions in additional exchange encounters (Prince et al. 1991; Freire et al. 2004; Lynch et al. 2012; DeCesar et al. 2015; Ridolfi et al. 2021, 2022; Kremer et al. 2022). If these massive companions are degenerate, these orbits retain the high eccentricity of the systems after the exchange encounters. Such systems could even include MSP–black hole binaries (e.g., Ye et al. 2019).

These systems are especially interesting because the rotational stability of MSPs, which rivals atomic clocks on long timescales (e.g., Hobbs et al. 2020) makes them extremely useful for a diverse array of applications: Their orbital eccentricities and large companion masses enable precise mass measurements for the MSPs and their companions (Lynch et al. 2012; Ridolfi et al. 2019) and, at least in one case so far, tests of gravity theories (Jacoby et al. 2006). Even if they are not in eccentric binaries, MSPs in globular clusters can be used to probe their gravitational potentials (Prager et al. 2017; Perera et al. 2017; Freire et al. 2017; Abbate et al. 2018).

M30 (NGC 7099) is a GC located at a distance of 8.1 kpc from the Sun, at Galactic coordinates $l = 27.^{\circ}18$, $b = -46.^{\circ}84$ (Harris 1996, 2010 revision), and has an estimated age of 12.9 Gyr (Forbes & Bridges 2010). This GC is of particular interest for pulsar searching as it is a core-collapsed cluster and has shown significant evidence of mass segregation (Howell et al. 2000). Its core has a radius of $3.''6$ and its half-light radius is $61.''8$ (Harris 2010).

Previous searches for pulsars in M30 using observations taken at the 100-m Green Bank Telescope (GBT), yielded the discovery of two radio pulsars: PSR J2140−2310A (M30A), an 11.01 ms eclipsing pulsar in a 4.17 hr orbit, and PSR J2140−2311B (M30B) (Ransom et al. 2004), a 13.0 ms binary pulsar. Based on the spin frequency evolution seen in the 7.8 hr discovery observation in 2001, Ransom et al. (2004) could infer that this pulsar must be in a highly eccentric ($e \geqslant 0.45$), relativistic orbit. However, a precise characterization of this orbit was not possible because the pulsar was not detected in any other observations made with the GBT with the total time spent on source adding up to 30 hr. The reason for this is that it was discovered while its flux was being amplified by diffractive scintillation, which produces a strong modulation in the flux densities of the pulsars in this cluster (see Figure 3 of Ransom et al. 2004, which shows the flux density variations observed for M30A). Because of this, the basic characteristics of this system have remained a mystery for the last 20 yr.

Aided by sensitivity gains offered by the MeerKAT telescope, we present the first set of detections of this pulsar since the discovery observation in 2001 that have revealed the nature of this system.

2. Observations and Data Reduction

We observed M30 using MeerKAT, with at least 56 antennas per observation, on nine occasions between 2020 December and 2022 September (see Table 1 for details). Our initial campaign consisted of four observations, each lasting 60 minutes, taken as part of the TRansients And PUlsars with Meerkat (TRAPUM;[11] Stappers & Kramer 2016) Large Survey Project (LSP) between 2020 December and 2021 January.

Of these, the first two observations were recorded with the *L*-band receivers, with a central frequency of 1284 MHz and a bandwidth of 856 MHz split into 4096 frequency channels and sampled every 76.56 μs. The next two observations were recorded with Ultra High Frequency (UHF) receivers, centered at the frequency of 816 MHz with a bandwidth of 544 MHz, also split into 4096 channels, and sampled every 60.24 μs. We used the Filterbanking Beamformer User Supplied Equipment (FBFUSE; Barr 2018) as the backend to form between 275 and 287 synthesized beams on the sky with an overlap fraction[12] of 0.8, enabling arcsecond localization of pulsars after initial detection. The beam-tiling pattern corresponding to each pointing was estimated based on an optimal hexagonal packing approach of elliptical beams. This was done using the MOSAIC[13] software (Chen et al. 2021). The beams were processed online by the Accelerated Pulsar Search User Supplied Equipment (APSUSE) computing cluster, where data from each beam are converted into an 8 bit, Stokes-*I* pulsar-search mode file, based on the SIGPROC FILTERBANK format (Lorimer 2011). We then incoherently dedispersed the observations offline, using a dispersion measure (DM) of 25.06 pc cm^{-3} (which corresponds to the DM of the other known pulsar, M30A), and then downsampled the data in frequency by a factor of 16 (bringing the total number of frequency channels to 256) so as to reduce the data volume.

Based on the results obtained from the TRAPUM observations, we also carried out a follow-up orbital campaign, with a pseudo-log cadence, between 2022 June and July. Each of these observations was 60 minutes, with the exception of a 280 minute (4.5 hr) periastron passage observation in September 2022. These follow-up observations were made using at least 60 antennas, the UHF receivers, and the Pulsar Timing User Supplied Equipment (PTUSE) backend (Bailes et al. 2020). PTUSE recorded the data from a single tied-array beam placed at the nominal center of M30.[14] The full bandwidth of 544 MHz was split into 1024 frequency channels, coherently dedispersed to a DM of 25.06 pc cm^{-3}, downsampled to 256 frequency channels, and saved in PSRFITS format (Hotan et al. 2004). PTUSE observations were also recorded in search mode since at the time we did not yet have an accurate orbital ephemeris and to allow further pulsar searches. These observations were recorded in full Stokes mode to enable polarimetric measurements and sampled every 15.06 μs for high-resolution pulsar timing.

All the observations used the Inter-Quartile Range Mitigation algorithm (Morello et al. 2022) as a first pass to filter out bright radio-frequency interference (RFI) signals. The data were then shipped on hard drives to Garching, Germany, where the primary search analysis was conducted using the Max Planck Computing and Data Facility (MPCDF) Hercules[15] cluster.

2.1. Search Analysis

Our search analysis consists of two pipelines implementing different search algorithms. First is PULSAR_MINER,[16] a user-

[11] http://www.trapum.org

[12] The boundary of the synthesized beams in the tiling overlap each other with the power level equal to this ratio.

[13] https://github.com/wchenastro/Mosaic

[14] Additionally, we also recorded TRAPUM search-mode observations in parallel to enable further pulsar and transient searches of the cluster.

[15] https://docs.mpcdf.mpg.de/doc/computing/clusters/systems/Radioastronomy.html

[16] https://github.com/alex88ridolfi/PULSAR_MINER

Table 1
List of MeerKAT Observations of M30B Recorded and Analyzed for This Work

Obs. ID	Start Time (Date)	Start Time (MJD)	Length (s)	Backend	t_{samp} (μs)	N_{pol}	f_c (MHz)	Δf (MHz)	N_{chan}	N_{ant}	N_{beam}
01L	2021 Dec 17	59200.512	3600	APSUSE	76.56	1	1284	856	4096	56	287
02L	2021 Dec 29	59212.572	3600	APSUSE	76.56	1	1284	856	4096	56	287
03U	2021 Jan 22	59236.453	3600	APSUSE	60.24	1	816	544	4096	56	287
04U	2021 Jan 30	59244.488	3600	APSUSE	60.24	1	816	544	4096	56	275
05U[a]	2022 Jun 29	59759.837	3600	PTUSE	9.41	4	816	544	1024	60	1
06U[a]	2022 Jun 30	59760.179	3600	PTUSE	9.41	4	816	544	1024	60	1
07U[a]	2022 Jun 30	59760.880	3600	PTUSE	9.41	4	816	544	1024	60	1
08U[a]	2022 Jul 2	59762.877	3600	PTUSE	9.41	4	816	544	1024	60	1
09U	2022 Sep 9	59831.785	16200	PTUSE	9.41	4	816	544	1024	64	1

Notes. t_{samp}: sampling time, N_{pol}: number of polarizations recorded, f_c: central frequency, Δf: bandwidth, $N_{ant:}$ number of MeerKAT antennas used, N_{beam}: number of tied-array beams recorded. All APSUSE observations were incoherently dedispersed to DM = 25.06 pc cm^{-3} and downsampled to 256 channel filterbank files. All PTUSE observations were recorded with full Stokes information, coherently dedispersed to a DM of 25.06 pc cm^{-3} and downsampled to 256 channel psrfits files to save disk space.

[a] These observations are phase connected in our timing solution provided in Table 2. The remaining observations have been fitted with arbitrary time offsets in the form of "JUMP" statements.

friendly wrapper of PRESTO,[17] which is a Fourier-domain acceleration search pipeline sensitive to binary pulsars in constant acceleration ($P_{orb} \gtrsim 10\,T_{obs}$; Ransom et al. 2002, 2003). Our second pipeline called 3D/5D_PEASOUP[18] uses the template-bank algorithm to search for pulsars in compact circular orbit binaries by coherently searching across three Keplerian parameters in the time domain (Balakrishnan et al. 2022).

Before commencing searching, we cleaned all of the observations again using PRESTO's `rfifind` program, which masks frequency channels and sub-integrations contaminated by RFI using appropriate user-defined thresholds. Additionally, we removed Fourier frequencies identified in a topocentric zero-DM time series as they are almost certainly caused by RFI. We then dedispersed the data between 23 and 28 pc cm^{-3} and transformed our observation frame of reference to the solar system barycenter by adding or subtracting appropriate delays from the dedispersed time series using the DE421 JPL Ephemerides (Folkner et al. 2009). We searched for both isolated and binary pulsars using the `accelsearch` routine in PRESTO. For our searches, we used the GPU version[19] of PRESTO with a $z_{max} = 1200$ and performed incoherent harmonic summing of up to 16 harmonics to be sensitive to narrow-duty cycle pulsars.

Additionally, in order to be sensitive to binary pulsars in more compact orbits, we performed the search not only on the full 60 minute observation but also split the data into 15 and 30 minute chunks and searched each segment with the same z_{max} value of 1200. This gives us extra sensitivity toward pulsars in compact orbits (i.e., $P_{orb} \gtrsim 150$ min for the 15 minute segments) at the cost of raising our minimum flux density limit as sensitivity improves with $T_{obs}^{1/2}$. These searches also improve our chances of finding a pulsar that shows significant diffractive scintillation.

Finally, in order to take advantage of the sensitivity offered by the full 60 minute observation, but increase our sensitivity toward compact orbits (i.e., not be limited to $P_{orb} \gtrsim 10\,T_{obs}$) we carried out a template-bank search (Messenger et al. 2009; Knispel 2011; Allen et al. 2013; Knispel et al. 2013) where we expand from a one-dimensional acceleration search to a three-dimensional Keplerian parameter search (orbital period, projected semimajor axis, and initial orbital phase) assuming a circular orbit binary. Here we searched for orbits between 4 and 10 hr in the 60 minute observation and between 2 and 5 hr in the 30 minute chunks, with an initial orbital phase between 0 and 2 π, mismatch of 10%, and a coverage of 90% assuming a minimum pulsar spin period of 2 ms, minimum pulsar mass of 1.4 $M_\odot$, and a maximum companion mass of 8 $M_\odot$. We refer interested readers to Section 3 of Ridolfi et al. (2021) and Section 2 of Balakrishnan et al. (2022) for a more in-depth review of the PULSAR_MINER and the 3D/5D_PEASOUP pipelines, respectively. On average, we folded approximately 350 pulsar candidates per beam for all our acceleration searches and 1000 pulsar candidates per beam for our template-bank searches.[20] Multiplying this number by the total number of synthesized beams times the four initial observations taken under the TRAPUM project, approximately 1.5 million pulsar candidates were produced, which was infeasible to inspect manually. Therefore, we used machine-learning-based pipelines to extract the most interesting pulsar candidates. We used the Pulsar Image Classification system (PICS; Zhu et al. 2014) and Pulsar Candidate Identification Using Semi-Supervised Generative Adversarial Networks (SGAN; Balakrishnan et al. 2021) and manually inspected candidates that scored above a threshold of 0.5 using either of these algorithms. This reduced our candidate viewing load from 1.5 million to approximately 5000 (~0.3%). No new pulsars have been discovered in our analysis. However, our pipelines blindly redetected and confirmed the elusive binary pulsar PSR J2140−2311B described in the next section.

3. Results

3.1. Confirmation of PSR J2140−2311B (M30B)

We redetected M30B in two out of four of our initial set of TRAPUM observations. Both of our detections were from data recorded in the UHF band taken during 2021 January 22 and 30

[17] https://github.com/scottransom/presto
[18] https://github.com/vishnubk/5D_Peasoup
[19] https://github.com/jintaoluo/presto_on_gpu

[20] Larger numbers of candidates are expected for higher-order template-bank searches since our computational trials scale up due to the addition of more binary parameters.

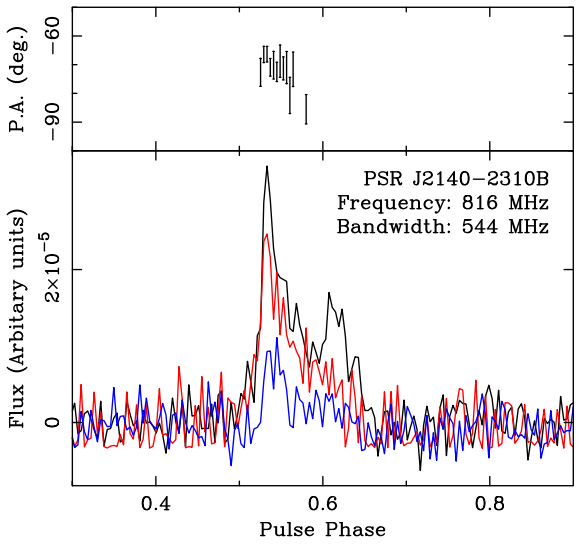

Figure 1. Bottom panel: high-S/N polarization pulse profile of M30B obtained by summing phase-connected observations between 05U and 08U recorded in the UHF band. The black line represents the total intensity, red and blue lines display the linear and circular polarization pulse profile, respectively. Top panel: measurements of position angle (PA) in degrees above 4σ of the linear polarization.

(obs id: 03U and 04U) with a folded significance of 12.4σ and 14.0σ, respectively. The measured barycentric spin period of 12.9896559(7) ms with a detected DM = 25.07 pc cm^{-3} in the January 22 observation immediately confirmed that this was indeed M30B initially reported in Ransom et al. (2004). The absence of any clear detection from searches in the L band is consistent with the result of most GBT observations.

M30B has been consistently detected in our follow-up orbital campaigns between 2022 June and September, which were recorded in the UHF band; this is likely caused by a combination of factors: the steep spectrum of the pulsar, the fact that scintles are narrower at these lower frequencies (thus leading to more of them being averaged within a given band), higher sensitivity of MeerKAT (Gain $G = 2.63$ K Jy^{-1}, assuming 60 antennas used) compared to GBT ($G = 2.0$ K Jy^{-1}) and the wider frequency bandwidth of the MeerKAT UHF receivers (bandwidth: 544 MHz) compared to the GBT 820 MHz receiver (bandwidth: 200 MHz). Using PTUSE full Stokes observations taken between 2022 June and July (obs ID: 05U-08U), we were able to obtain a high-signal-to-noise ratio (S/N) polarization pulse profile of this pulsar using standard routines in the PSRCHIVE[21] (van Straten et al. 2012) software suite. We detected a rotation measure (RM) = 8 ± 6 rad m^{-2}, which was used to de-Faraday the folded archive to produce a linear and circular polarization pulse profile. This is shown in Figure 1.

3.2. Localization

The FWHM of the GBT beam at 20 cm is about 9′. When M30B was initially discovered, its position within the GBT telescope beam and by extension within the cluster was not yet known. The position of a pulsar with respect to the cluster center gives us important clues regarding the evolutionary history of the system. As mentioned in Section 2, MeerKAT observations of this cluster made with the TRAPUM backend typically consist of over 270 synthesized beams (hereafter referred to as coherent beams) on the sky. These beams are much smaller than the typical sky area observed by a single-dish radio telescope at the same frequency. For example, the size[22] of the semimajor and semiminor axes of the coherent beam during the beginning of the January 22nd UHF band were 27.″3 and 21.″9, respectively[23] Therefore, a detection in one of the beams already tells us that the pulsar is within or very near that beam. This position measurement can be improved further if detections in multiple beams are available which was the case with M30B where we detected the pulsar in five neighboring beams in the 2021 January 22nd observation. We used the SEEKAT multibeam localiser software[24] (Bezdenhout et al. 2022) to improve our estimate for the position of this pulsar. SEEKAT takes in the position of the coherent beam, the detected S/N within it, and the beam point-spread function (PSF) calculated using the software MOSAIC and performs a maximum-likelihood analysis to get a better estimate of the pulsar's position. In Figure 2, we show the known radio timing position of M30A and the recently localized M30B's position within the cluster along with the TRAPUM beam-tiling pattern for the beginning of the observation taken on 2021 January 22. M30B is located 1.2 (1)′ away from the cluster center and just outside the half-light radius. The consequences of this in terms of the evolutionary history of M30B are discussed in Section 3.5.

3.3. Preliminary Orbital Analysis

Given our new detections from TRAPUM and MEERTIME observations, the first step was to obtain an accurate orbital solution for M30B, which requires the identification of its orbital period P_b. In order to do this, we extracted the barycentric epoch and spin period corresponding to each detection. We then used a modified version[25] of the Bhattacharyya & Nityananda (2008) roughness algorithm to get an initial estimate of the orbital period of this system. Roughness ϕ is calculated by folding the data with a number of trial P_b values. For each iteration, we then obtain data for the observed spin period versus the orbital phase. From this, we compute the summation of the squared differences of the observed spin period between adjacent values of ϕ. The idea here is that the roughness should be minimum for the correct value of P_b. Building on the original algorithm, we added a variance measure to obtain a more robust measurement of P_b. Using this method, we estimated the P_b of M30B to be 6.215 days. This estimate was then used as an initial guess to build a first-pass orbital ephemeris using the program FITORBIT.[26]

3.4. Pulsar Timing

The next step was to improve this orbital ephemeris through a process known as pulsar timing. We started by folding all our observations using the DSPSR[27] software package (van Straten & Bailes 2011) modulo the predicted spin period from the orbital ephemeris obtained from FITORBIT. Then we formed a

[21] https://psrchive.sourceforge.net/

[22] Defined here with an elliptical fit at 50% of the power level.

[23] The size of the coherent beam depends on the configuration of the antennas used, on the central frequency of the observation, and on the source elevation.

[24] https://github.com/BezuidenhoutMC/SeeKAT

[25] https://github.com/mcbernadich/CandyCracker

[26] https://github.com/vivekvenkris/fitorbit

[27] https://dspsr.sourceforge.net/

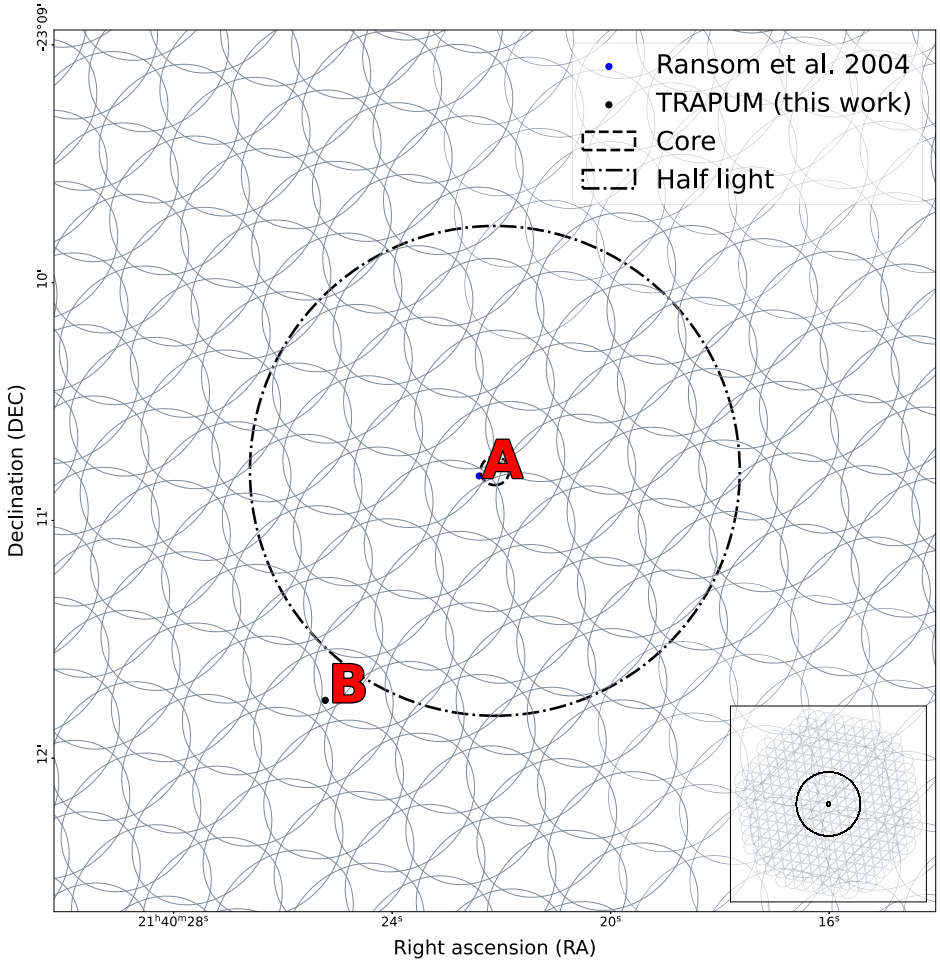

Figure 2. Beam-tiling pattern at the start of the TRAPUM observation of M30 recorded in the UHF band on 2021 January 22. The boundary of the ellipse plotted here corresponds to 50% of the maximum power level. The beam pattern was generated using MOSAIC. The boundaries of the core and half-light radius have been obtained from the Harris (2010) catalog, which are marked as dashed and dashed–dotted lines, respectively. Overlaid on the plots in red are the two known pulsars within this cluster both of which were reported in Ransom et al. (2004). While M30A was discovered and regularly monitored since then, M30B remained undetected since the discovery detection and has now finally been confirmed, localized, and solved using TRAPUM. The inset shows a zoomed-out version of the same plot.

stable integrated pulse profile by summing the data in frequency, time, and polarization. We then cross-correlated this high-S/N pulse profile with an analytic template to extract times of arrival (TOAs) at our telescope site for a particular rotational phase of the pulsar. These preprocessing steps were done using standard routines from the PSRCHIVE[28] (van Straten et al. 2012) software suite.

Using TOAs derived from our MeerKAT detections, we were able to determine the orbital parameters of M30B using the software TEMPO[29] and the theory-independent "DD" model (Damour & Deruelle 1986). To get a better estimate of the DM, we extracted TOAs per frequency channel by summing each observation in time and polarization and averaging our data across frequencies from 256 to 4 frequency channels. These TOAs were then used to fit for DM by keeping all other orbital and spin parameters fixed using TEMPO. Our ephemeris was precise enough to fold and detect the pulsar in the 2021 and 2022 UHF observations (obs id: 03U–08U). However, since this ephemeris is not a phase-connected solution, a priori we do not yet know the rotation count between groups of TOAs of different observations. This is estimated by adding an arbitrary time offset for each observation in the form of "JUMP" statements between each set of locally connected TOAs and then attempting to establish the rotation counts between close sets of observations, as described in detail in Section 3 of Freire & Ridolfi (2018). Given the general sparsity of the detections, especially between 2001 and 2022, we could not connect all observations this way, so we used DRACULA (described in Section 4 of Freire & Ridolfi 2018) to automatically identify the unknown number of rotations between observations. However, even with this algorithm, we cannot yet determine a unique phase-coherent timing solution for all the data of the pulsar, as the number of observations is still too small for that.

However, we obtained a good orbital solution (see Table 2, $\chi^2 = 1.36$) that can fold all the observations, including the early 2001 observation, and another observation taken during periastron on 2022 September (obs ID: 09U). Additionally, all the TOAs from the 4 day orbital campaign (obs ID: 05U-08U) made in 2022 are phase connected; this provides an important contribution to the precision of our solution. The postfit residuals for this model can be found in Figure 3 with the arbitrary time offsets subtracted. The flat residuals indicate that the model provides, within its current limitations, a good description of the timing. We were also able to recover the pulsar in one of our MEERKAT *L*-band observations

[28] https://psrchive.sourceforge.net/
[29] https://tempo.sourceforge.net/

Table 2
Timing Parameters for PSR J2140−2311B (M30B) Presented in Barycentric Dynamical Time (TDB)

Pulsar	J2140−2311B
Fitting program	TEMPO
Time units	TDB
Terrestrial time standard	UTC(NIST)
Solar system ephemeris	DE440
R.A., α (J2000)	21:40:25.2(3)
decl., δ (J2000)	−23:11:45(7)
Spin frequency, f (Hz)	76.9833055(6)
First-spin frequency derivative, $\dot{f}$ (Hz s^{-1})	$3(15) \times 10^{-15}$
Reference epoch (MJD)	59763.520924
Start of timing data (MJD)	52161.993
End of timing data (MJD)	59831.942
Dispersion measure, DM (pc cm^{-3})	25.063(3)
Number of TOAs	73
Residuals rms (μs)	39.42
Binary Parameters	
Binary model	DD
Projected semimajor axis, x_p (lt-s)	19.5222(7)
Orbital eccentricity, e	0.87938(2)
Longitude of periastron, ω (deg)	160.8007(4)
Epoch of periastron passage, T_0 (MJD)	59763.520649(6)
Rate of periastron advance, $\dot{\omega}$ (deg/yr)	0.078(2)
Orbital period, P_b (days)	6.21565400(6)
Derived Parameters	
Galactic longitude, l (°)	27.161(1)
Galactic latitude, b (°)	−46.851(2)
Total system mass, $M_{\rm TOT}$ ($M_\odot$)	2.53(8)
Companion mass, M_c ($M_\odot$)	$\geqslant$1.10
Pulsar mass, M_p ($M_\odot$)	$\leqslant$1.43
Spin period, P (s)	0.01298982933(2)
First-spin period derivative, $\dot{P}$ (s s^{-1})	$-6(25) \times 10^{-19}$
Mass function, $f(M_p)$ ($M_\odot$)	0.2067
Total offset from GC center, $\theta_\perp$ (arcmin)	1.2(1)

Notes. For R.A. and decl., we report the values that correspond to the maximum likelihood reported by SEEKAT along with their 1σ uncertainty. Both the position and DM have been kept fixed for our timing analysis given the sparsity of our detections.

(obs ID: 02L), which was undetected by our blind searches. However, even with the aid of this ephemeris, we still could not recover the signal in any of the old GBT observations besides the discovery observation, nor in two 30 minute observations of M30 at a frequency of 400 MHz taken with the Giant Metrewave Radio Telescope (GMRT) in India as part of the GC survey presented by Gautam et al. (2022).

These nondetections can be explained because we do not yet have a phase-coherent timing solution, but also because of the difference of sensitivity of the MeerKAT, GBT, and GMRT observations. The survey sensitivity of TRAPUM GC observations for NGC 1851 has been reported previously in Section 2.1 of Ridolfi et al. (2022) using the modified radiometer equation (Dewey et al. 1985). Adjusting these numbers for the values reported in Table 1 for TRAPUM observations of M30, we get a minimum detectable flux density of 14.1 μJy at the L band and 19.9 μJy at the UHF band compared to 109.3 μJy for the 400 MHz GMRT observation of M30 reported in Gautam et al. (2022). Ransom et al. (2004) reported that the GBT observations of M30 were sensitive to normal millisecond pulsars in the range of ∼50–100 μJy.

An important parameter in this orbital solution is the system's rate of advance of periastron, which we measure to be $\dot{\omega} = 0.078 \pm 0.002$ deg yr^{-1}. The precision of this measurement greatly benefits from the inclusion of the 2001 TOAs, even with the fit of an arbitrary time offset. Using the DDGR model (Taylor 1987; Taylor & Weisberg 1989), which assumes that general relativity (GR) accounts for the relativistic effects observed in the timing, the total mass of the system derived from $\dot{\omega}$ is $M_{\rm tot} = 2.53 \pm 0.08\, M_\odot$. The mass–mass diagram assuming GR along with our measurement of $\dot{\omega}$ is shown in Figure 4. In this figure, we can see that by combining the total mass measurement with the constraint from the mass function, we can estimate a minimum companion mass of 1.10 $M_\odot$ and a maximum pulsar mass of 1.43 $M_\odot$.

Note that, although our measurement of the first-spin frequency derivative $\dot{f}$ is not significant, it is important to fit for this parameter in order to obtain a realistic uncertainty for $\dot{\omega}$. Indeed, if we do not fit for $\dot{f}$, the uncertainty of $\dot{\omega}$ will be one order of magnitude smaller. Assuming the small $\dot{f}$ typical of MSPs is not warranted because it could have a significant contribution from the system's acceleration in the cluster.

3.5. System Origin

Most binary MSPs in our Galaxy are in highly circularised orbits with a low-mass He-WD or a nondegenerate or semidegenerate ultralight companion ($M_c \leqslant 0.08\, M_\odot$, Tauris et al. 2012 and references within). These systems are highly recycled ($P \leqslant 10$ ms) due to the long mass transfer phase, which transfers matter and angular momentum from the companion to the pulsar, spinning it up to very rapid rates and reducing the magnetic field strengths of the NS (Bhattacharya & van den Heuvel 1991; Bhattacharya 2002; Tauris & van den Heuvel 2006). Intermediate spin-period pulsars ($10 \leqslant P \leqslant 20$ ms, Camilo et al. 2001) tend to have massive CO or ONeMg WD companions (e.g., PSR J1802−2104, Ferdman et al. 2010), but their orbits still have very low eccentricities.

If the companion star is massive enough to undergo its own supernova (SN) explosion and if the binary orbit survives, then a double NS system (DNS; see Tauris et al. 2017 for a review) will form. These systems tend to be mildly recycled ($P \geqslant 17$ ms; see Stovall et al. 2018) as their massive companions do not live for long, halting the recycling process earlier. Unlike systems with WD companions, they have highly eccentric orbits because of the kick and mass loss from the second SN (Brandt & Podsiadlowski 1995; Tauris et al. 2017).

Given its high orbital eccentricity, M30B could in principle have formed like the DNSs in the Galactic disk. The total mass is similar to that of the lightest known DNS systems (like PSRs J1411+2551 and J1946+2052; Martinez et al. 2017; Stovall et al. 2018). However, this scenario is unlikely given the spin period of M30B—$P \sim 12.98$ ms, faster than for any pulsars in a DNS seen to date in the Galaxy. Furthermore, there are currently no massive stars in GCs that would provide a second SN; the last time these existed in GCs was more than 10 Gyr ago. Thus, if M30B was such a primordial DNS, its characteristic age (τ_c) would have to be at least ∼10 Gyr. We note, though, that given the large γ of the host cluster, it is very unlikely that the system would still resemble its original configuration.

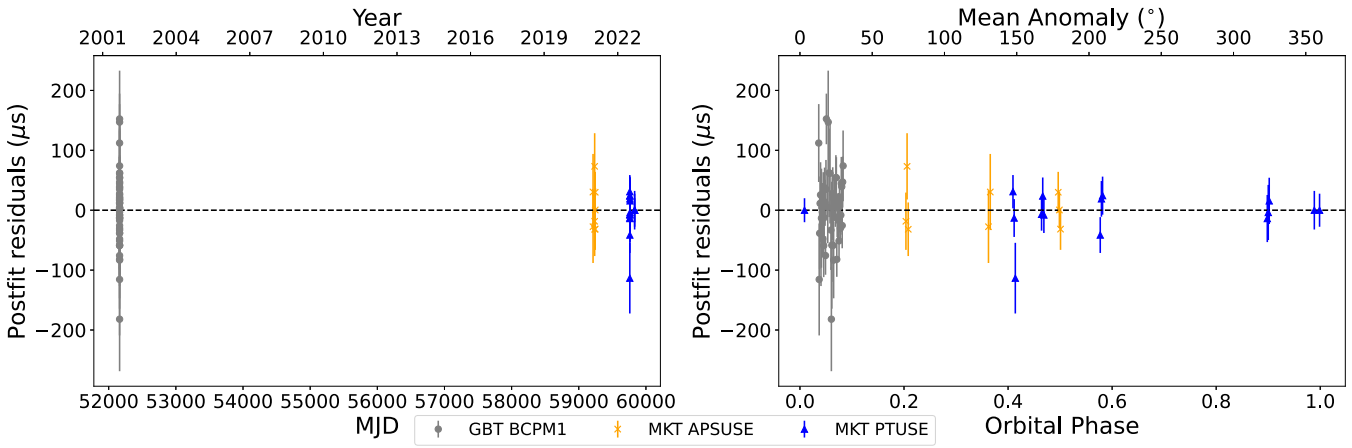

Figure 3. Postfit timing residuals of PSR J2140−2311B as a function of time and orbital phase using the DD Binary model. Colors indicate different telescopes and backends used to obtain the TOAs.

The spin period of M30B is more compatible with a relatively massive CO or ONeMg WD companion. In the Galactic disk, these systems have low orbital eccentricities, but given the large number of stellar encounters in GCs, the orbital eccentricity could have been greatly increased (Phinney 1992). Thus, it is possible that the companion is a massive WD star whose progenitor recycled the pulsar; in this case we should also expect $\tau_c \sim 10$ Gyr.

A more likely hypothesis is that M30B is a result of an exchange encounter, where the lighter star that recycled the pulsar was ejected during the binary's chaotic encounter with a more massive degenerate star, which is the current companion. Given the random dynamics of such an encounter, we cannot decide on the nature of the companion—either a massive WD or an NS—based on arguments from stellar evolution (although massive WDs are generally more likely given their larger abundance in the cluster; see, e.g., Ye et al. 2019; Kremer et al. 2021).

Several eccentric MSP binaries with massive companions have recently been found in core-collapsed GCs (which have the highest γ values: PSR J1807−2500B in NGC 6544 (Lynch et al. 2012), PSR J1835−3259A in NGC 6652 (DeCesar et al. 2015), and PSR J1823−3021G in NGC 6624 (Ridolfi et al. 2021)). These are thought to be exchange products because their spin periods are very small compared to binary pulsars in the Galactic disk with similarly massive companions. In all core-collapsed GCs, these systems represent approximately one-third of the known population of binary radio pulsars. For this calculation, we have adopted the definition of core-collapsed GC from the Harris catalog (Harris 1996, 2010 revision) and only considered binary pulsars with well-measured orbits. We then assume that pulsars in an eccentric orbit ($e > 0.1$) orbiting a massive companion ($m_c > 0.38\,M_\odot$) are likely to be the result of exchange products. Using this definition and the updated numbers from the "GC Pulsar catalog," we find that 5 out of the 14 (∼35.7%) binary pulsars in core-collapsed GCs are likely to be exchange products; in non-core-collapsed GCs only 10 out of 109 (∼9.2%) binary pulsars fulfill these criteria. The location of M30B in a core-collapsed GC is thus an indication that it likely originated in an exchange encounter. Another clue is its high eccentricity: Among secondary exchange products, M30B has the third-highest orbital eccentricity after PSR J1835−3259A ($e \sim 0.96$; DeCesar et al. 2015) and PSR J0514−4002A ($e \sim 0.88$; Freire et al. 2007; Ridolfi et al. 2019).

When exchange encounters are very frequent, they might even happen during the LMXB phase. In this case, the recycling process is truncated, resulting in a partially recycled pulsar that still has a relatively high magnetic field and will therefore appear young. Unlike MSPs, such mildly recycled pulsars spin down fast, which means that their LMXB disruption must be recent. This explains why slow, apparently young pulsars in GCs are overwhelmingly found in high-γ GCs and lie below the pulsar spin-up line (Verbunt & Freire 2014; Abbate et al. 2022), although in this regard we must keep in mind that there are alternative explanations for the formation of apparently young pulsars in GCs (e.g., Ivanova et al. 2008).

The recent disruption of an LMXB by a massive degenerate intruder that then becomes the pulsar's companion is a likely explanation for the parameters of PSR B2127+11C ($P = 30.5$ ms and $\tau_c \sim 0.1$ Gyr), a binary pulsar located in the core-collapsed GC M15. Although this system superficially resembles a Galactic DNS (see Andrews & Mandel 2019), its characteristic age—less than 1% of the age of the GC—is too small for it to be a DNS formed from the primordial population of massive stars of M15 (Prince et al. 1991). If the recent disruption of an LMXB is the explanation for the relatively slow spin of M30B, then we might also expect the pulsar to have a characteristic age much smaller than the age of the M30 GC itself.

One clue that suggests that PSR B2127+11C was recently involved in an exchange encounter is its large distance (0.94′) from the center of M15 (Prince et al. 1991; Jacoby et al. 2006). Normally, mass segregation causes the pulsar population in dense GCs to be very centrally condensed, with most pulsars within, or near their cores (e.g., Freire et al. 2017; Prager et al. 2017; Abbate et al. 2018). This is the case for all other pulsars in M15 (Anderson 1993) and for M30A (Ransom et al. 2004). The large distance of PSR B2127+11C from the center of M15 is possibly the result of the recoil caused by the ejection of the previous light companion that partially recycled the pulsar; the time elapsed since the recoil (∼0.1 Gyr, if it is the same event that disrupted the LMXB) is presumably too short for the system to have migrated back to the center of the GC via dynamical friction. Interestingly, M30B is located 1.2(1)′ from the cluster center and just outside its half-light radius, which again suggests a recent

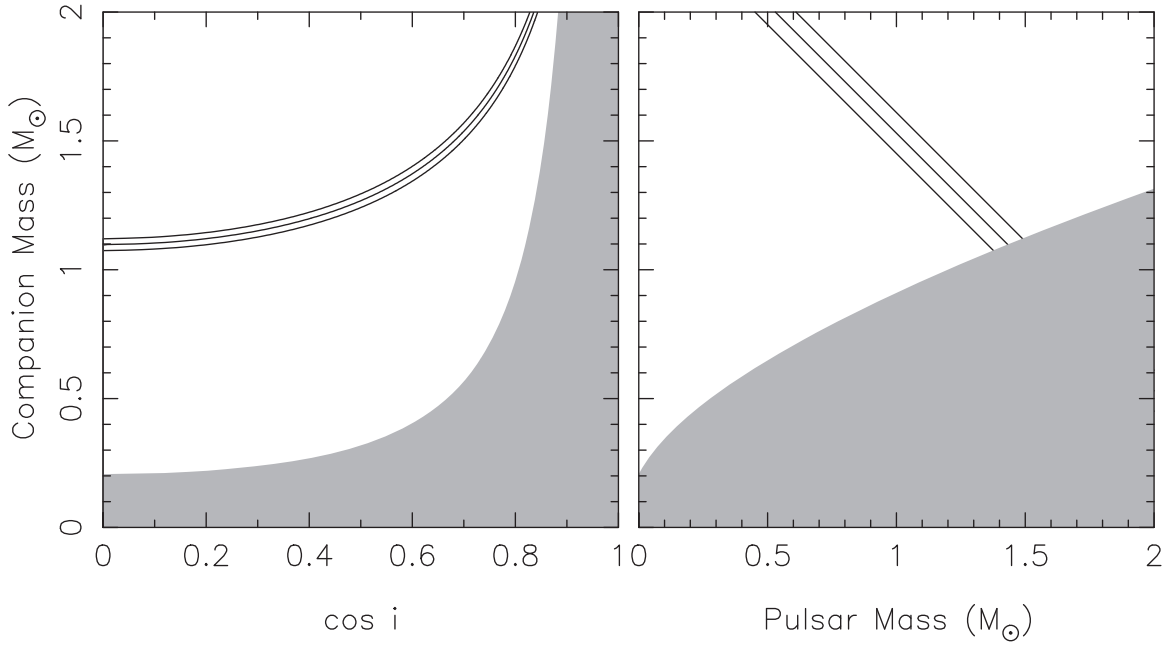

Figure 4. Mass–mass diagram of M30B assuming GR obtained from pulsar timing. In the left plot, we show the mass of the companion M_c vs. the cosine of the inclination angle. The gray region here is excluded by the requirement that $M_p > 0$. On the right, we present M_c vs. the mass of the pulsar M_p. The gray region is excluded by the mass function and orbital geometry (i.e., $\sin i \leqslant 1$). The black triplet of lines shows the regions consistent with the measurement of the advance of periastron $\dot{\omega}$ along with their 1σ uncertainty. As we can see, from these measurements we can derive an upper limit for M_p and a lower limit for M_c.

exchange interaction. Overall, pulsars with such large distances from the center (in core radii) occur more often in high-γ GCs (Verbunt & Freire 2014).

3.6. Prospects

We plan to continue timing M30B as part of the MeerTime GC pulsar timing program. These observations are necessary in order to fully connect all the MeerKAT observations (possibly all the way back to 2001) and shed light on the nature of the M30B system. A phase-coherent timing solution will yield much improved astrometric, spin, and orbital parameters. The spin and orbital period derivatives will be extremely important because their measurement will allow the determination of τ_c, which will be crucial for distinguishing between a primordial binary with a massive companion or a more recent exchange product. This will also greatly improve all orbital parameters, especially P_b and $\dot{\omega}$.

The following step will be to determine the individual masses via the detection of additional relativistic effects. Dense orbital campaigns in the near future might lead to the detection of the Shapiro delay (Shapiro 1964): For an inclination angle of 60°, the h_3 parameter (Freire & Wex 2010) would be 1.2 μs. This can be detected with 2σ significance with 4000 ToAs with the current timing precision. The parameter will be larger (and therefore detected with higher significance) for higher inclinations; another possibility is to somehow improve the timing precision. If the orbital inclination is low and/or we are unable to improve the timing precision, then we will have to wait to detect the Einstein delay. However, the longitude of periastron ω of M30B is not optimal for this goal (see detailed discussion in Ridolfi et al. 2019), so if the Shapiro delay is not detectable, measuring the component masses with the Einstein delay will take several decades.

4. Conclusion

In this Letter, we presented the confirmation of M30B with the first set of new detections of this pulsar since its discovery in 2001. We found that the pulsar can be reliably detected with the MeerKAT UHF receivers; this has finally allowed, 20 yr after the discovery, a detailed characterization of this system: It is located 1.2(1)′ from the cluster center and the pulsar is in a highly eccentric ($e = 0.879$) orbit around a companion that could either be a massive WD or an NS. We also measured the rate of periastron advance, which indicates a total system mass consistent with that of the lightest known DNSs in our Galaxy (Martinez et al. 2017; Stovall et al. 2018).[30] M30B was likely formed as the result of a secondary exchange encounter, similar systems have been observed in other GCs with very dense cores. Further timing observations are necessary to obtain a phase-connected timing solution for this pulsar, which would yield much improved astrometric, spin and orbital parameters. Continued timing might result in the detection of additional relativistic effects and the determination of the individual masses of the components. The characterization of M30B is a demonstration of the unrivaled sensitivity of MeerKAT for radio sources in the Southern celestial hemisphere.

The MeerKAT telescope is operated by the South African Radio Astronomy Observatory, which is a facility of the National Research Foundation, an agency of the Department of Science and Innovation. SARAO acknowledges the ongoing advice and calibration of GPS systems by the National Metrology Institute of South Africa (NMISA) and the time-space reference systems department of the Paris Observatory. PTUSE was developed with support from the Australian SKA Office and Swinburne University of Technology. MeerTime

[30] For a list of NS mass measurements, see https://www3.mpifr-bonn.mpg.de/staff/pfreire/NS_masses.html.

data is housed on the OzSTAR supercomputer at Swinburne University of Technology. The OzSTAR program receives funding in part from the Astronomy National Collaborative Research Infrastructure Strategy (NCRIS) allocation provided by the Australian Government. The authors also acknowledge MPIfR funding to contribute to MeerTime infrastructure. TRAPUM observations used the FBFUSE and APSUSE computing clusters for data acquisition, storage and analysis. These clusters were funded and installed by the Max-Planck-Institut für Radioastronomie and the Max-Planck-Gesellschaft. The National Radio Astronomy Observatory is a facility of the National Science Foundation operated under cooperative agreement by Associated Universities, Inc. The Green Bank Observatory is a facility of the National Science Foundation operated under cooperative agreement by Associated Universities, Inc. V.B., A.R., E.D.B., F.A., D.J.C., W.C., P.C.C.F., T. G., M.K., P.V.P., and V.V.K. acknowledge continuing valuable support from the Max-Planck Society. V.B. gratefully acknowledges support from ERC Synergy Grant "BlackHoleCam" Grant Agreement Number 610058. S.M.R. is a CIFAR Fellow and is supported by the NSF Physics Frontiers Center awards 1430284 and 2020265. This work is supported by the Max-Planck Society as part of the "LEGACY" collaboration on low-frequency gravitational wave astronomy. A.R. and A.P. gratefully acknowledge financial support by the research grant "iPeska" (P.I. Andrea Possenti) funded under the INAF national call Prin-SKA/CTA approved with the Presidential Decree 70/2016. A.R. and A.P. also acknowledge support from the Ministero degli Affari Esteri e della Cooperazione Internazionale—Direzione Generale per la Promozione del Sistema Paese—Progetto di Grande Rilevanza ZA18GR02. B.W.S. acknowledges funding from the European Research Council (ERC) under the European Union's Horizon 2020 research and innovation program (grant agreement No. 694745). Pulsar research at UBC is supported by an NSERC Discovery Grant and by the Canadian Institute for Advanced Research.

ORCID iDs

Vishnu Balakrishnan https://orcid.org/0000-0003-3244-2711
Paulo C. C. Freire https://orcid.org/0000-0003-1307-9435
S. M. Ransom https://orcid.org/0000-0001-5799-9714
Alessandro Ridolfi https://orcid.org/0000-0001-6762-2638
E. D. Barr https://orcid.org/0000-0001-8715-9628
W. Chen https://orcid.org/0000-0002-6089-7943
Vivek Venkatraman Krishnan https://orcid.org/0000-0001-9518-9819
D. Champion https://orcid.org/0000-0003-1361-7723
M. Kramer https://orcid.org/0000-0002-4175-2271
T. Gautam https://orcid.org/0000-0002-8396-2197
Prajwal V. Padmanabh https://orcid.org/0000-0001-5624-4635
Yunpeng Men https://orcid.org/0000-0003-4137-4247
F. Abbate https://orcid.org/0000-0002-9791-7661
B. W. Stappers https://orcid.org/0000-0001-9242-7041
I. Stairs https://orcid.org/0000-0001-9784-8670
E. Keane https://orcid.org/0000-0002-4553-655X
A. Possenti https://orcid.org/0000-0001-5902-3731

References

Abbate, F., Possenti, A., Ridolfi, A., et al. 2018, MNRAS, 481, 627
Abbate, F., Ridolfi, A., Barr, E. D., et al. 2022, MNRAS, 513, 2292
Allen, B., Knispel, B., Cordes, J. M., et al. 2013, ApJ, 773, 91
Alpar, M. A., Cheng, A. F., Ruderman, M. A., & Shaham, J. 1982, Natur, 300, 728
Anderson, S. B. 1993, PhD thesis, California Institute of Technology
Andrews, J. J., & Mandel, I. 2019, ApJL, 880, L8
Bailes, M., Jameson, A., Abbate, F., et al. 2020, PASA, 37, e028
Balakrishnan, V., Champion, D., Barr, E., et al. 2021, MNRAS, 505, 1180
Balakrishnan, V., Champion, D., Barr, E., et al. 2022, MNRAS, 511, 1265
Barr, E. D. 2018, in IAU Symp. 337, Pulsar Astrophysics the Next Fifty Years, ed. P. Weltevrede et al. (Cambridge: Cambridge Univ. Press), 175
Bezdenhout, M. C., Clark, C. J., Breton, R. P., et al. 2022, RASTI, submitted
Bhattacharya, D. 2002, JApA, 23, 67
Bhattacharya, D., & van den Heuvel, E. P. J. 1991, PhR, 203, 1
Bhattacharyya, B., & Nityananda, R. 2008, MNRAS, 387, 273
Brandt, N., & Podsiadlowski, P. 1995, MNRAS, 274, 461
Camilo, F., Lyne, A. G., Manchester, R. N., et al. 2001, ApJL, 548, L187
Camilo, F., & Rasio, F. A. 2005, in ASP Conf. Ser. 328, Binary Radio Pulsars, 328, ed. F. A. Rasio & I. H. Stairs (San Francisco, CA: ASP), 147
Chen, W., Barr, E., Karuppusamy, R., Kramer, M., & Stappers, B. 2021, JAI, 10, 2150013
Clark, G. W. 1975, ApJL, 199, L143
Damour, T., & Deruelle, N. 1986, AnHP, 44, 263
Davies, M. B., & Benz, W. 1995, MNRAS, 276, 876
Davies, M. B., Benz, W., & Hills, J. G. 1992, ApJ, 401, 246
Davies, M. B., & Hansen, B. M. S. 1998, MNRAS, 301, 15
DeCesar, M. E., Ransom, S. M., Kaplan, D. L., Ray, P. S., & Geller, A. M. 2015, ApJL, 807, L23
Dewey, R. J., Taylor, J. H., Weisberg, J. M., & Stokes, G. H. 1985, ApJL, 294, L25
Ferdman, R. D., Stairs, I. H., Kramer, M., et al. 2010, ApJ, 711, 764
Folkner, W. M., Williams, J. G., & Boggs, D. H. 2009, IPNPR, 42, 1
Forbes, D. A., & Bridges, T. 2010, MNRAS, 404, 1203
Freire, P. C., Gupta, Y., Ransom, S. M., & Ishwara-Chandra, C. H. 2004, ApJL, 606, L53
Freire, P. C. C., Ransom, S. M., & Gupta, Y. 2007, ApJ, 662, 1177
Freire, P. C. C., & Ridolfi, A. 2018, MNRAS, 476, 4794
Freire, P. C. C., Ridolfi, A., Kramer, M., et al. 2017, MNRAS, 471, 857
Freire, P. C. C., & Wex, N. 2010, MNRAS, 409, 199
Gautam, T., Ridolfi, A., Freire, P. C. C., et al. 2022, A&A, 664, A54
Harris, W. E. 1996, AJ, 112, 1487
Harris, W. E. 2010, arXiv:1012.3224
Hobbs, G., Guo, L., Caballero, R. N., et al. 2020, MNRAS, 491, 5951
Hotan, A. W., van Straten, W., & Manchester, R. N. 2004, PASA, 21, 302
Howell, J. H., Guhathakurta, P., & Tan, A. 2000, AJ, 119, 1259
Ivanova, N., Heinke, C. O., Rasio, F. A., Belczynski, K., & Fregeau, J. M. 2008, MNRAS, 386, 553
Ivanova, N., Rasio, F. A., Lombardi, J. C. J., Dooley, K. L., & Proulx, Z. F. 2005, ApJL, 621, L109
Jacoby, B. A., Cameron, P. B., Jenet, F. A., et al. 2006, ApJL, 644, L113
Knispel, B. 2011, PhD thesis, Albert Einstein Institute, Hannover; Leibniz University, Hannover
Knispel, B., Eatough, R. P., Kim, H., et al. 2013, ApJ, 774, 93
Kremer, K., Rui, N. Z., Weatherford, N. C., et al. 2021, ApJ, 917, 28
Kremer, K., Ye, C. S., Kıroğlu, F., et al. 2022, ApJL, 934, L1
Lorimer, D. R. 2011, SIGPROC: Pulsar Signal Processing Programs, Astrophysics Source Code Library, ascl:1107.016
Lynch, R. S., Freire, P. C. C., Ransom, S. M., & Jacoby, B. A. 2012, ApJ, 745, 109
Manchester, R. N., Hobbs, G. B., Teoh, A., & Hobbs, M. 2005, AJ, 129, 1993
Martinez, J. G., Stovall, K., Freire, P. C. C., et al. 2017, ApJL, 851, L29
Messenger, C., Prix, R., & Papa, M. A. 2009, PhRvD, 79, 104017
Morello, V., Rajwade, K. M., & Stappers, B. W. 2022, MNRAS, 510, 1393
Perera, B. B. P., Stappers, B. W., Lyne, A. G., et al. 2017, MNRAS, 468, 2114
Phinney, E. S. 1992, RSPTA, 341, 39
Prager, B. J., Ransom, S. M., Freire, P. C. C., et al. 2017, ApJ, 845, 148
Prince, T. A., Anderson, S. B., Kulkarni, S. R., & Wolszczan, A. 1991, ApJL, 374, L41
Ransom, S. M. 2008, in IAU Symp. 246, Dynamical Evolution of Dense Stellar, ed. E. Vesperini, M. Giersz, & A. Sills (Cambridge: Cambridge Univ. Press), 291
Ransom, S. M., Cordes, J. M., & Eikenberry, S. S. 2003, ApJ, 589, 911
Ransom, S. M., Eikenberry, S. S., & Middleditch, J. 2002, AJ, 124, 1788
Ransom, S. M., Stairs, I. H., Backer, D. C., et al. 2004, ApJ, 604, 328
Ridolfi, A., Freire, P. C. C., Gautam, T., et al. 2022, A&A, 664, A27
Ridolfi, A., Freire, P. C. C., Gupta, Y., & Ransom, S. M. 2019, MNRAS, 490, 3860
Ridolfi, A., Gautam, T., Freire, P. C. C., et al. 2021, MNRAS, 504, 1407

Shapiro, I. I. 1964, PhRvL, 13, 789
Sigurdsson, S., & Phinney, E. S. 1995, ApJS, 99, 609
Stappers, B., & Kramer, M. 2016, in MeerKAT Science: On the Pathway to the SKA,Vol. 277 (Trieste Sissa), 9
Stovall, K., Freire, P. C. C., Chatterjee, S., et al. 2018, ApJL, 854, L22
Tauris, T. M., Kramer, M., Freire, P. C. C., et al. 2017, ApJ, 846, 170
Tauris, T. M., Langer, N., & Kramer, M. 2012, MNRAS, 425, 1601
Tauris, T. M., & van den Heuvel, E. P. J. 2006, in Compact Stellar X-Ray Sources, ed. W. Lewin & M. van der Klis, Vol. 39 (Cambridge: Cambridge Univ. Press), 623
Taylor, J. H. 1987, General Relativity and Gravitation, Vol. 20 (Cambridge: Cambridge Univ. Press), 209
Taylor, J. H., & Weisberg, J. M. 1989, ApJ, 345, 434
van den Berg, M. 2020, in IAU Symp. 351, Star Clusters: From the Milky Way to the Early, ed. A. Bragaglia et al. (Cambridge: Cambridge Univ. Press), 367
van Straten, W., & Bailes, M. 2011, PASA, 28, 1
van Straten, W., Demorest, P., & Oslowski, S. 2012, AR&T, 9, 237
Verbunt, F., & Freire, P. C. C. 2014, A&A, 561, A11
Verbunt, F., & Hut, P. 1987, in IAU Symp. 125, The Origin and Evolution of Neutron Stars, ed. D. J. Helfand & J. H. Huang (Cambridge: Cambridge Univ. Press), 187
Ye, C. S., Kremer, K., Chatterjee, S., Rodriguez, C. L., & Rasio, F. A. 2019, ApJ, 877, 122
Ye, C. S., Kremer, K., Rodriguez, C. L., et al. 2022, ApJ, 931, 84
Zhu, W. W., Berndsen, A., Madsen, E. C., et al. 2014, ApJ, 781, 117